III-Antimonide/Nitride Based Semiconductors for Optoelectronic Materials and Device Studies LDRD 26518 Final Report

Gregory M. Peake, John F. Klem, Terry W. Hargett, Darwin K. Serkland, Michael J. Cich, Normand A. Modine, Karen E. Waldrip, Steven R. Kurtz, Andrew A. Allerman, Eric Daniel Jones

Sandia National Laboratories

III-Antimonide/Nitride Based Semiconductors for Optoelectronic Materials and Device Studies LDRD 26518 Final Report

Gregory M. Peake, John F. Klem, Terry W. Hargett,
Darwin K. Serkland, and Michael J. Cich
RF Microsystems Technologies Department

Normand A. Modine
Nanostructure & Semiconductor Physics Department

Karen E. Waldrip, and Steven R. Kurtz
Semiconductor Materials & Device Sciences Department

Andrew A. Allerman
Chemical Processing Science Department

Eric Daniel Jones
Semiconductor Materials & Device Sciences Department

Sandia National Laboratories
P.O. Box 5800
Albuquerque, New Mexico 87185-0601

Abstract

The goal of this LDRD was to investigate III-antimonide/nitride based materials for unique semiconductor properties and applications. Previous to this study, lack of basic information concerning these alloys restricted their use in semiconductor devices. Long wavelength emission on GaAs substrates is of critical importance to telecommunication applications for cost reduction and integration into microsystems. Currently InGaAsN, on a GaAs substrate, is being commercially pursued for the important 1.3 micrometer dispersion minima of silica-glass optical fiber; due, in large part, to previous research at Sandia National Laboratories. However, InGaAsN has not shown great promise for 1.55 micrometer emission which is the low-loss window of single mode optical fiber used in transatlantic fiber. Other important applications for the antimonide/nitride based

materials include the base junction of an HBT to reduce the operating voltage which is important for wireless communication links, and for improving the efficiency of a multijunction solar cell. We have undertaken the first comprehensive theoretical, experimental and device study of this material with promising results. Theoretical modeling has identified GaAsSbN to be a similar or potentially superior candidate to InGaAsN for long wavelength emission on GaAs. We have confirmed these predictions by producing emission out to 1.66 micrometers and have achieved edge emitting and VCSEL electroluminescence at 1.3 micrometers. We have also done the first study of the transport properties of this material including mobility, electron/hole mass, and exciton reduced mass. This study has increased the understanding of the III-antimonide/nitride materials enough to warrant consideration for all of the target device applications.

Table of Contents

1. Introduction

Dilute nitride semiconductor materials have been a discriminating technology at Sandia National Laboratories since their development. Many of the theoretical, materials properties and device implementations for InGaAsN were first realized at SNL. This has lead to commercialization of device applications such as vertical cavity surface emitting lasers (VCSEL) operating near 1.3 µm. Long wavelength VCSELs in the range of 1.3 – 1.55 µm could potentially revolutionize communication technology due to the high efficiency, excellent beam quality and manufacturability of VCSELs. Current promising long wavelength VCSEL materials, based on InGaAsN or GaAsSb, are both grown on GaAs substrates where the superior thermal conductivity and index contrast of AlGaAs DBR mirrors can be employed. However, because of poor valence or conduction band alignments, these systems do not satisfy the needed temperature stability and it is unlikely that these systems will produce VCSELs with wavelengths > 1.3 µm in the near future. The GaAsSbN material system may be a superior candidate for the 1.3-1.55 µm semiconductor laser system because it offers independent control of the valence and conduction band alignments and can be engineered to span a range of bandgaps from 0.8 to 1.2 eV (1.55 - 1 µm).
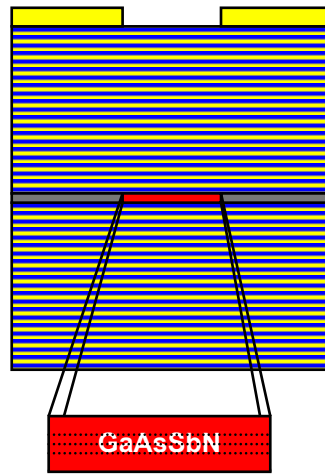
Figure 1. VCSEL with GaAsSbN active region for 1.3-1.55 µm emission.

The base layer of an NPN heterojunction bipolar transistor (HBT) would also benefit from a high valence band offset, which is easily designed using the GaAsSbN material system.
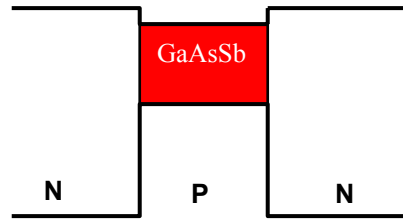
Figure 2. NPN Heterojunction Bipolar Transistor with GaAsSbN base region.

Multijunction solar cells are yet another device application that would benefit from the ability of the quaternary GaAsSbN to both lattice match the underlying substrate and provide an appropriate energy gap for increased efficiency.
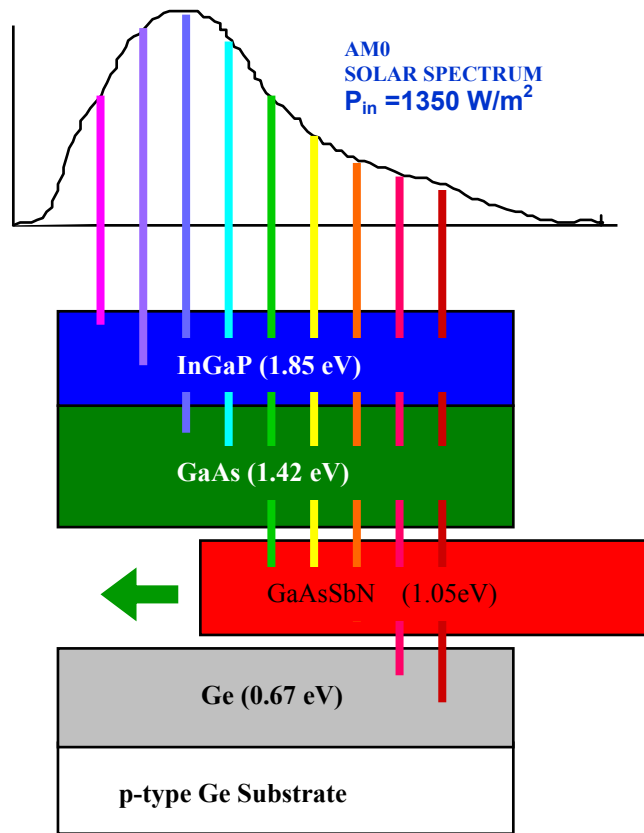
Figure 3. Multijunction Solar Cell with 1.05 eV GaAsSbN for improved efficiency.

Previous to this study, lack of basic information concerning this alloy restricted its use in semiconductor devices. Therefore, we have attempted to thoroughly investigate the GaAsSbN alloy system. This report summarizes the results of a combined theoretical and experimental study of GaAsSbN.

2. Theoretical Studies of Sb/N Materials

Significant theoretical understanding of the III-Sb/N material properties was accomplished during the course of this study. Early work concentrated on the differences between the pressure dependent behavior of candidate III-V alloys allowing us to concentrate on the more promising systems. First principles bandstructure calculations predicted photoluminescence properties, bandgap fluctuations, clustering effects, and relative incorporation of constituents.

Initial work focused on studying the dependence of band gap on composition and pressure for the GaBAs and GaAsSb alloys. Our results for concentration dependence (Fig. 4) show that as boron is added to GaAs, the band gap increases by a modest amount. For the case of an artificially ordered alloy (boron atoms are placed as far apart as possible), replacing 6.3% of the gallium atoms in GaAs with boron increases the band gap by almost 0.15 eV. Since this amount of boron also decreases the lattice constant by 0.9%, this increase in bandgap could, in principle, be compensated by adding additional indium to BInGaAsN alloys lattice matched to a GaAs substrate. However, this additional indium would likely further degrade minority carrier mobility and device performance. In contrast, in our calculations, replacing 6.3% of the arsenic atoms in GaAs with antimony decreases the band gap of the artificially ordered alloy by 0.10 eV (Fig. 5), while increasing the lattice constant by 0.5%. Similar calculations for InGaAs with 6.3% indium indicate that the band gap is reduced by 0.08 eV, while the lattice constant is increased by 0.4%. This suggests that antimony should be an effective alternative to indium as an additive to GaAsN used to further lower the band gap while matching to the GaAs lattice constant.
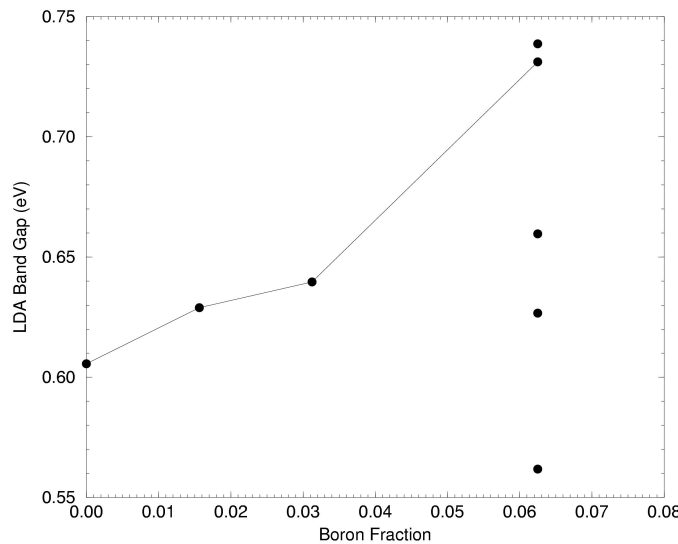

Figure 4. LDA band gap of GaBAs as a function of boron concentration. The multiple points at 6% indicate the range of values that can be obtained by varying the distance between two boron atoms.
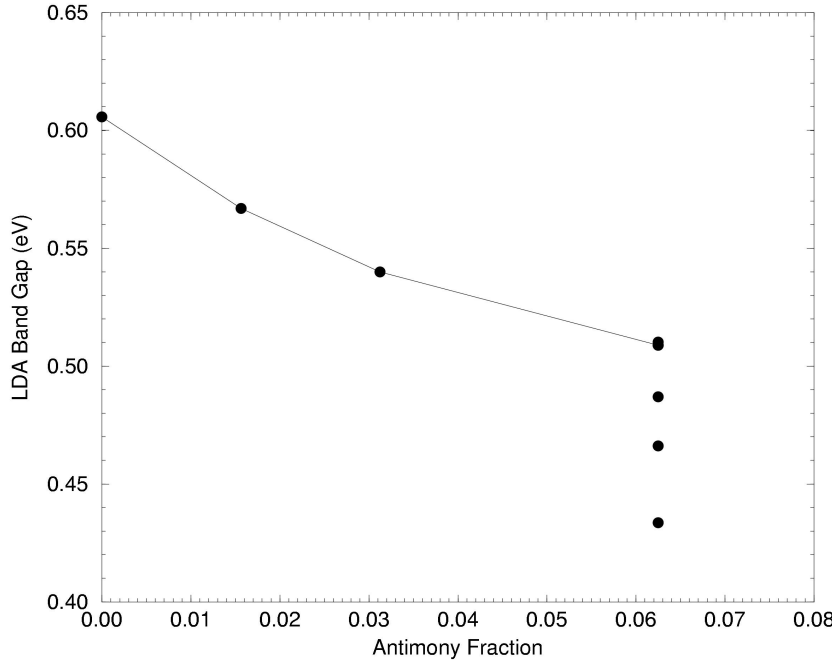
Figure 5. LDA band gap of GaAsSb as a function of antimony concentration. The multiple points at 6% indicate the range of values that can be obtained by varying the distance between two antimony atoms.

Following our fruitful theoretical work on GaAsN [1], we have studied the pressure dependence of the bands of GaBAs and GaAsSb with 3.1% of the minority component. The main conclusion of this work is that GaAsSb behaves similarly to GaAsN, while the behavior of GaBAs shows significant differences. In general, the addition of any third species to GaAs will reduce the symmetry of the system folding bands into the same point in the Brillouin zone and lifting degeneracies. This allows interactions between bands that were formerly forbidden by symmetry. However, the exact way in which this happens differs between GaBAs and GaAsSb. In particular, as we previously observed in GaAsN, the addition of Sb splits the triplet associated with the X-point of the GaAs conduction band into a singlet and a doublet (Fig. 6). Since the X-point moves down with pressure, while the gamma point moves up, this results in an avoided crossing between the gamma-like singlet and the X-like singlet. This results in a non-linear dependence of the band gap on pressure and a gradual decrease in photoluminescence (PL) signal strength as the conduction band minimum changes from gamma-like character to X-like character. In contrast, the three-fold degeneracy of the GaAs X-point is not lifted by the addition of boron (Fig. 7). Therefore, as in GaAs, a real crossing of the gamma-like and X-like states occurs with pressure. This results in a nearly piecewise linear (increasing below the crossing and decreasing above) dependence of the band gap on pressure. Since optical transitions become forbidden above the crossing, we can also expect to see a sudden disappearance of PL signal.

9

**Figure 6. LDA band energies of ordered GaAsSb
as a function of pressure. Energies are relative to the top of the valence band.**
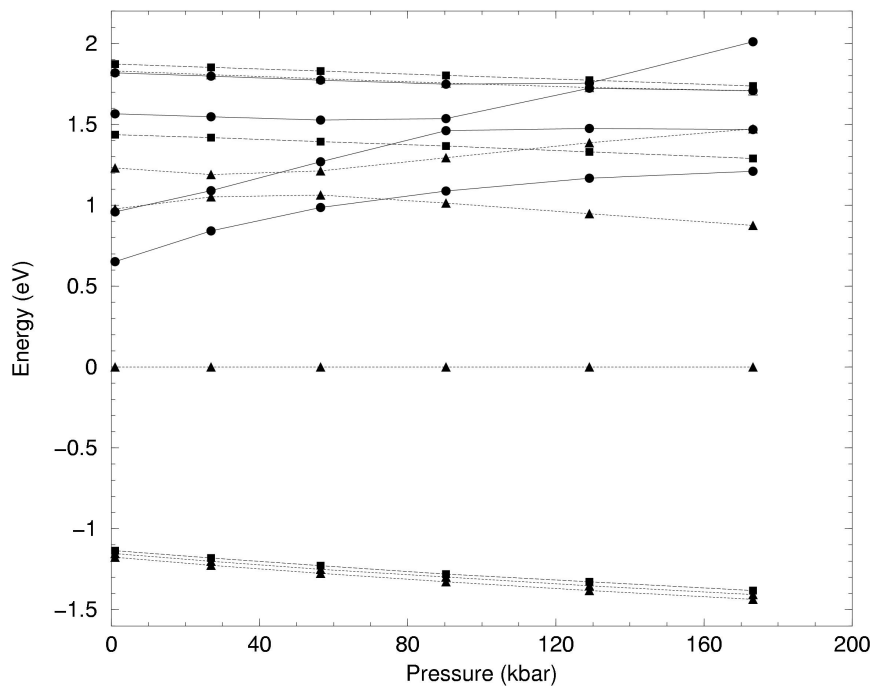
**Figure 7. LDA band energies of ordered GaBAs
as a function of pressure. Energies are relative to the top of the valence band.**

10

The symmetry arguments used above are technically only valid for ordered substitutions that occur on some superlattice with cubic symmetry, but we hypothesized that the amount of anti-crossing in mixed group-III alloys should generally be very small. In order to confirm this and get results that could be compared to experiment, we performed band structure calculations for AlGaAs and GaAsSb containing 16% Al (Sb) in a disordered configuration. Results are shown in Fig. 8 and Fig. 9. In agreement with our predictions, we found less than 20 meV of band repulsion in AlGaAs, compared with more than 100 meV of band repulsion in GaAsSb. These results demonstrate that there is a generic difference between the pressure dependent behavior of mixed group-III and mixed group-V zincblende III-V alloys

Figure 8. Lowest conduction band energies of disordered AlGaAs as a function of pressure. Energies are relative to the top of the valence band.
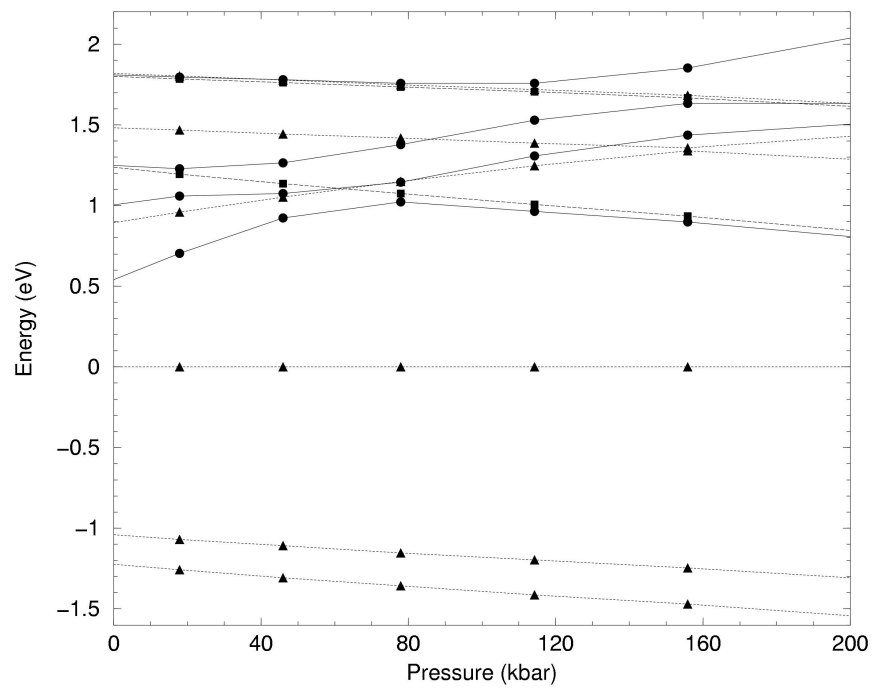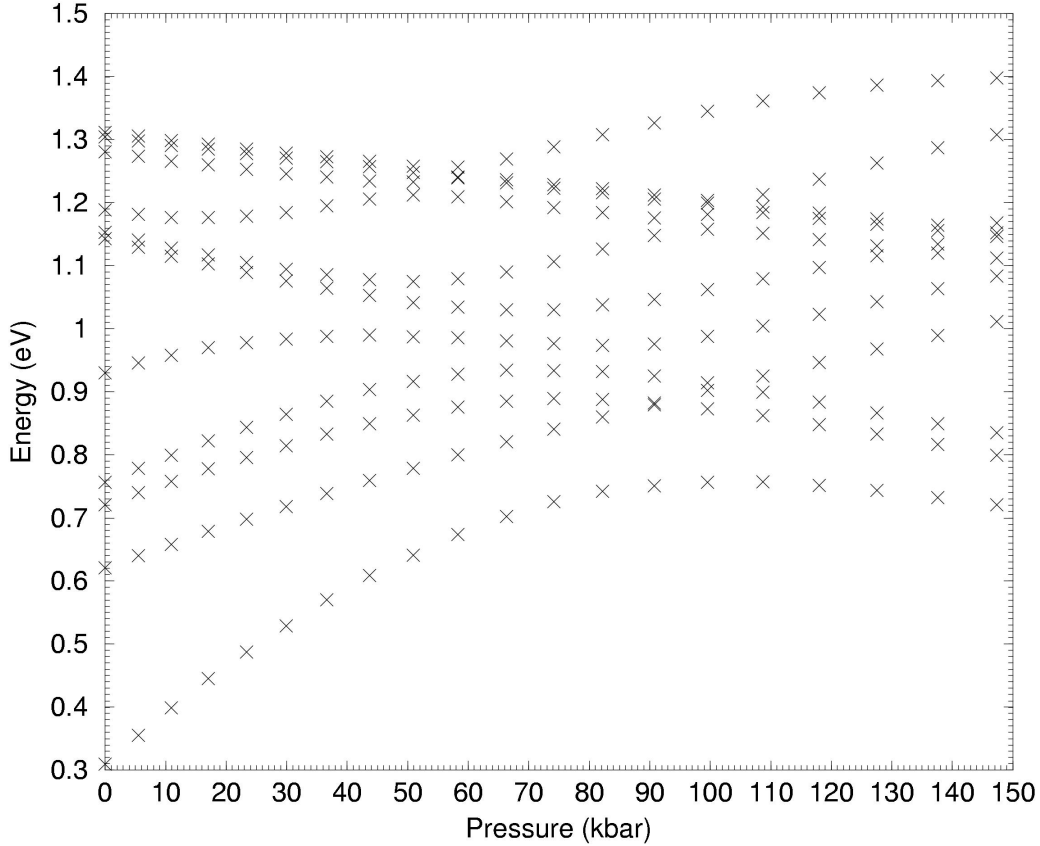
Figure 9. Lowest conduction band energies of disordered GaAsSb as a function of pressure. Energies are relative to the top of the valence band.

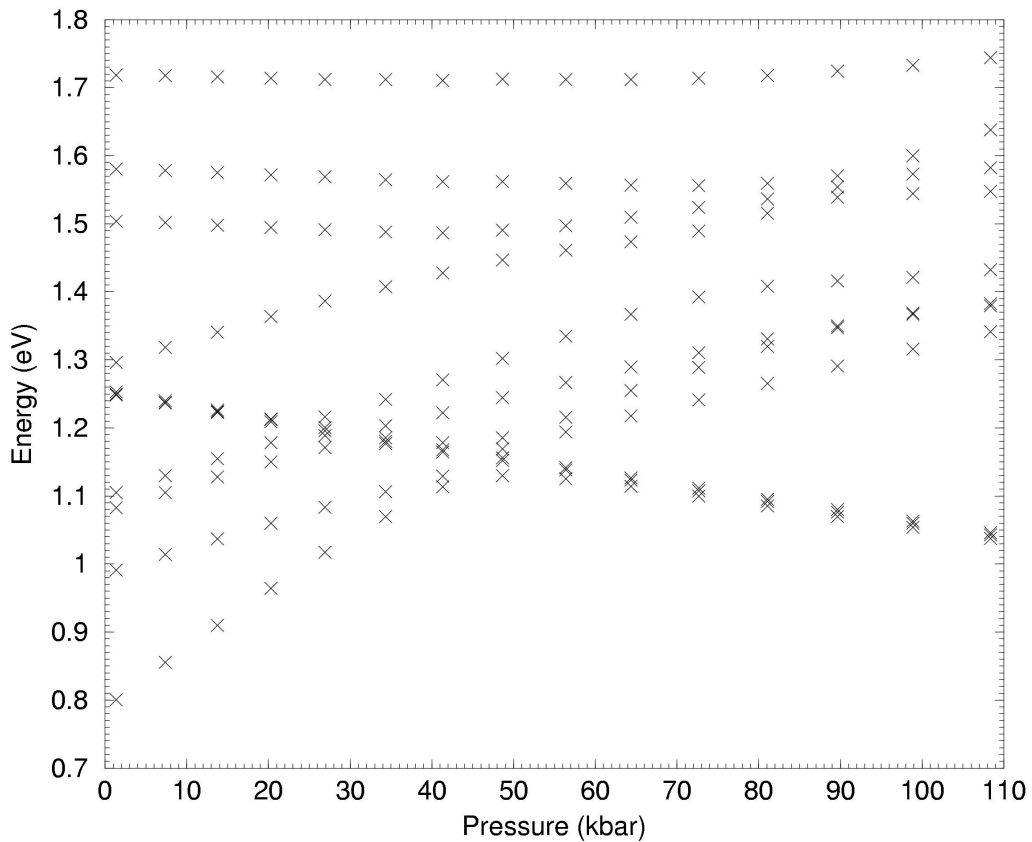We also studied clustering effects in GaBAs and GaAsSb. This was done by placing two atoms of the minority component in a 64 atom system (creating a 6.3% alloy) and varying the distance between these atoms. The main conclusion of these calculations is that boron atoms interact more strongly than antimony atoms. This difference in interaction strength is seen in both the band gap and the total energy of the system. Depending on the distance between minority component atoms, the band gap of 6.3% boron GaBAs varies by almost 0.2 eV, while the total energy varies by more than 0.3 eV (Fig. 10 and Fig. 11). In contrast, the band gap GaAsSb with 6.3% antimony varies by less than 0.08 eV, while the total energy varies by less that 0.1 eV (Fig. 12 and Fig. 13). These results suggest that carrier localization due to clustering and/or composition fluctuations may be less of a problem in GaAsSb than in GaBAs. In both systems, the band gap is an oscillating function of neighbor distance with minima at 1st and 4th neighbor distances. Also, in both systems, minima of the band gap correspond to maxima of the total energy (unfavorable configurations), and vice versa. Therefore, if the bulk alloy is able to equilibrate, thermodynamics may tend to suppress the configurations that most strongly trap carriers leading to better transport properties than would be expected from a purely random configuration.

12

Figure 10. LDA band gap of GaBAs as a function of the distance between two boron atoms in a cell.

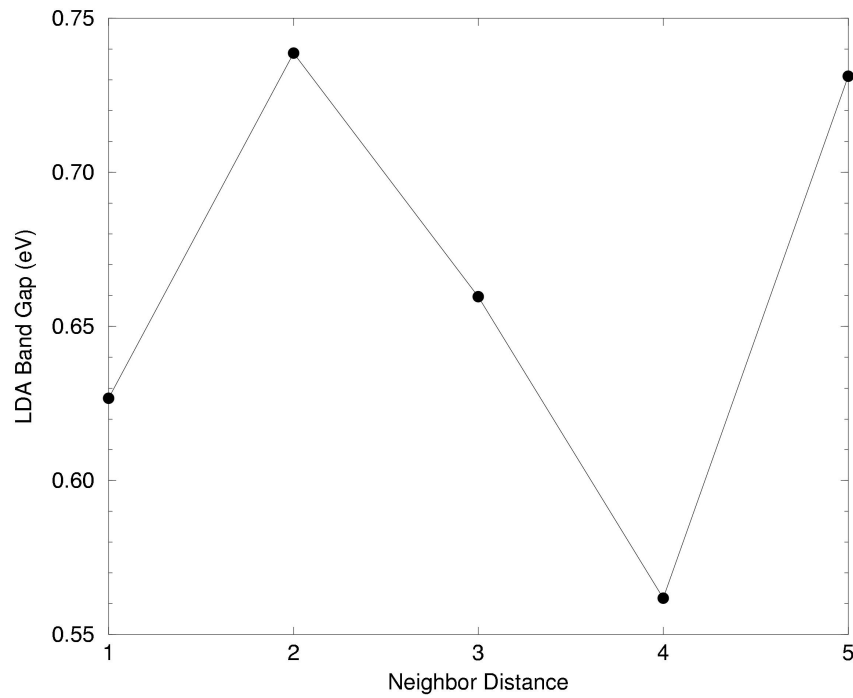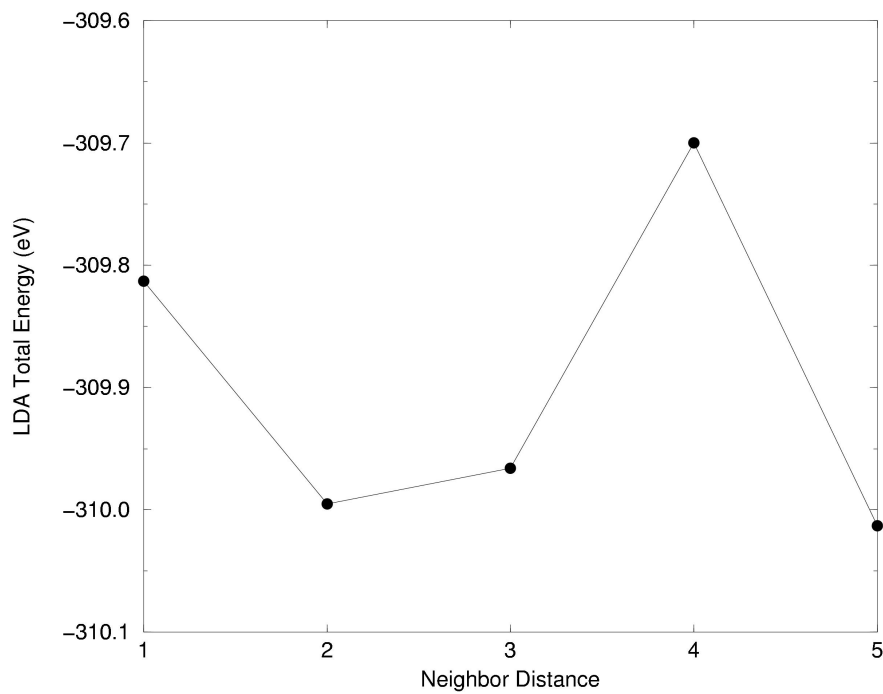**Figure 11. GaBAs total energy as a function of distance between two boron atoms in a cell.**
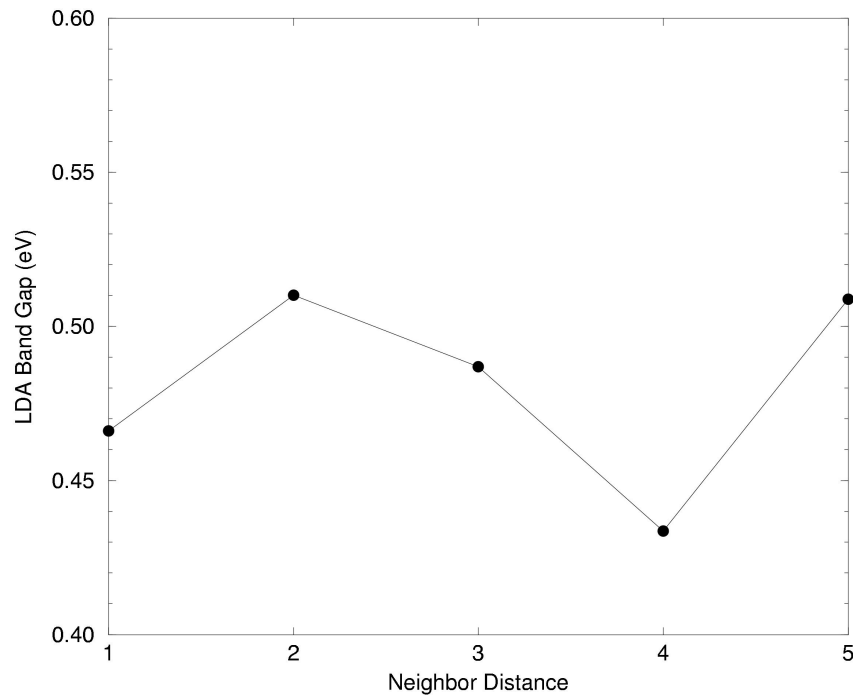
**Figure 12. LDA band gap of GaAsSb as a function of distance between
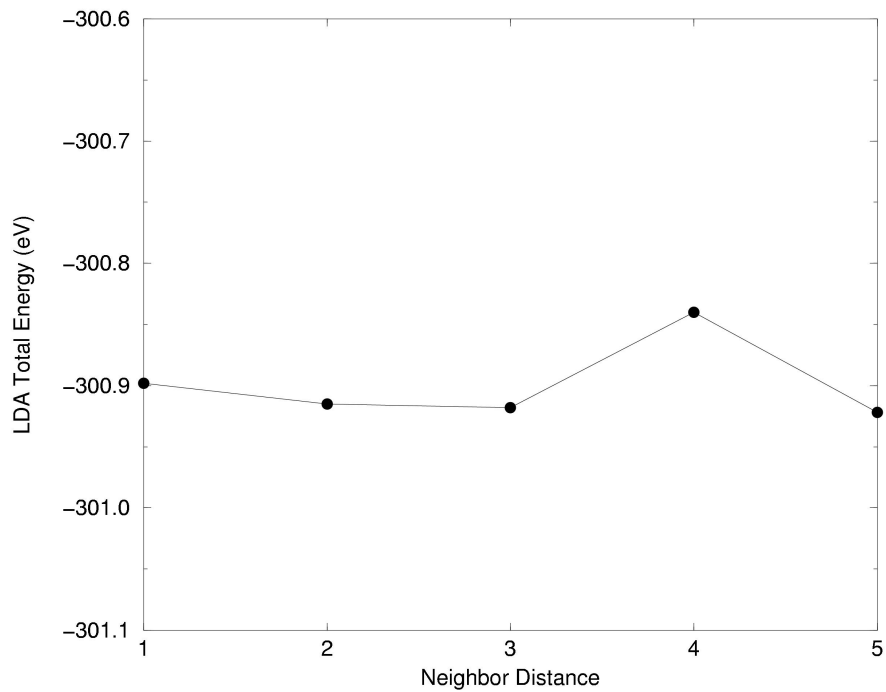two antimony atoms in a cell.**

**Figure 13. GaAsSb total energy as a function of distance between
two antimony atoms in a cell.**

The above band structure calculations for GaAsSb and InGaAs suggest that GaAsSbN would be an interesting alternative to InGaAsN. To confirm this hypothesis, we have performed band structure calculations for GaAsSbN and InGaAsN. In our calculations, we substituted one N atom and either an Sb or In atom on appropriate lattice sites of a GaAs cell. We also studied cells with two N atoms as a reference system. The effects of clustering were investigated by varying the distance between the substitution sites. Each cell was fully relaxed using first-principles forces. The results of these calculations are summarized in Fig. 14. The main conclusion of these calculations is that, at the same concentration, the band gaps of GaAsSbN and InGaAsN are the same to within the fluctuation in band gap given by different substitution sites. This variation in band gap was somewhat larger for GaAsSbN (0.16 eV) than for InGaAsN (0.10 eV). Although these band gap changes are larger than those in GaAsSb and InGaAs (0.08 eV and 0.03 eV, respectively), they are dwarfed by the fluctuation in band gap associated with N-N distance (0.47 eV). This suggests that band gap fluctuations in the mixed anion nitrides arise primarily from the configuration of the nitrogen atoms. The variation of the total energy with the distance between substitution sites is also important since low energy configurations are more likely to occur in thermodynamic equilibrium. The strongest variation in total energy occurred in the InGaAsN system, where a first neighbor In-N distance is favored over longer distances by 0.2-0.3 eV. This suggests that clusters of In and N atoms may be thermodynamically favorable in InGaAsN.
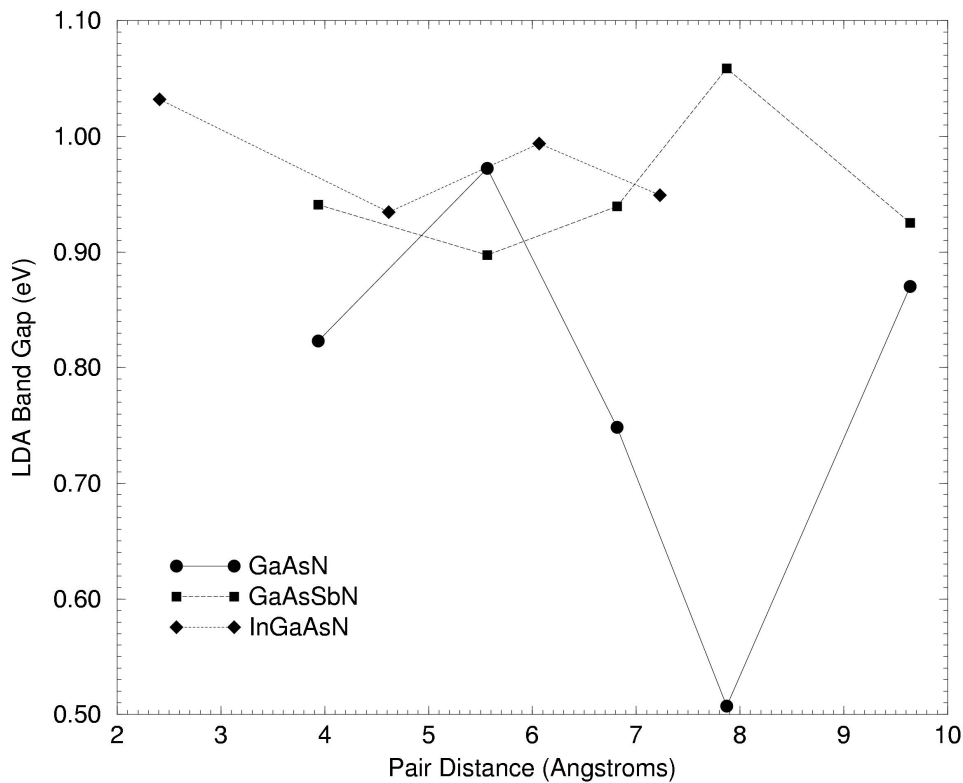

**Figure 14. LDA band gaps of GaAsN, GaAsSbN, and InGaAsN
as a function of the distance between the nitrogen atom and
the other minority species for a unit cell.**

Finally, we performed some preliminary calculations investigating N incorporation at Sb covered surfaces. It has been shown that the solubility of N in GaAs is enhanced (beyond the equilibrium bulk solubility) due to surface effects [2]. However, antimony acts as a surfactant during III-V epitaxial growth and covers the surface thoroughly before incorporating into the bulk. Therefore, there is no guaranty that surface effects will enhance nitrogen solubility when antimony is present. We investigated this issue theoretically. For a simplified model reconstruction of the Sb covered GaAs surface, we substituted a N atom at various sites below the surface, and compared the resulting total energies to those obtained for a clean GaAs surface. We concluded that a simple physical model could explain the results: The enhancement of N solubility at GaAs surfaces is due to the lower energy of the relatively small N atoms when they are substituted in compressively strained locations under the surface dimers of the reconstructed surface. The dimer bond length of Sb is longer, so it introduces less strain in the subsurface locations. We have verified this reduction of subsurface strain for the full reconstructions of similar Sb covered systems [3,4]. Therefore, we decided that our model system calculations were adequate to predict that covering the surface with Sb reduces the driving force for enhanced N solubility, and under otherwise identical conditions, we should expect somewhat reduced nitrogen incorporation in the presence of Sb.

3. Organometallic Vapor Phase Epitaxy of GaAsSbN Materials

This study produced the first OMVPE growth of GaAsSbN documented in the literature. Room temperature photoluminescence with a wavelength > 1.4 um was observed with electroluminescence at 1.3 um. The first measurements of Hall mobility, undertaken in this study, exhibited similar results to InGaAsN for the GaAsSbN system and similar background carrier concentrations. Preliminary measurements of the transport properties of GaAsSbN were also undertaken and found to be similar to InGaAsN.

3.1 Source Selection
1,1 -dimethylhydrazine (DMHy) was chosen over NH3 for this application due to the lower dissociation temperature and higher vapor pressure. However, using DMHy for the growth of InGaAsN causes the wafer surface temperature to cool down at high flow and DMHy is known to have batch-to-batch inconsistencies. TMGa and arsine were chosen for their compatibility with standard laser growths. Both TMSb and TESb have been explored for the growth of GaAsSbN. There was no evidence of N incorporation with TESb using x-ray diffraction (XRD) and PL. Figure 15 shows the XRD measurement of an attempt to grow GaAsSbN with TESb and TMSb. In both cases the results indicate a reduction in the apparent Sb concentration evidenced by the higher angle shift of the low angle envelope. In the TMSb growth, the PL shifts to longer wavelength, from 1.16 to 1.29 μm with the addition of DMHy. However for the TESb growth the PL shifts to shorter wavelength from 1.28 to 1.01 μm. This indicates a possible pre-reaction that inhibits incorporation of nitrogen species in the TESb chemistry.
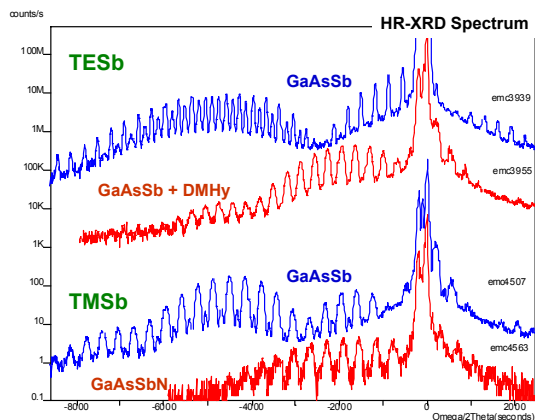
Figure 15. XRD of attempts to incorporate nitrogen into GaAsSb grown with TESb and TMSb. The PL of the TESb growth shifts to shorter wavelength indicating no N incorporation, while the TMSb growth shifts to longer wavelength indicating N incorporation.

3.2 OMVPE Growth Studies

There are fundamental differences in the OMVPE growth of antimonides with respect to arsenides, phosphides, and nitrides including lower melting points, the low equilibrium vapor pressure of Sb, and lack of a stable hydride of Sb which make GaAsSbN growth challenging. [5] OMVPE is typically carried out in the mass transport limited regime where there is a weak dependence on temperature; however, because of the lower growth temperatures used to incorporate nitrogen in GaAsSbN, the growth may be limited by kinetics. As shown in Figure 16, the growth of GaAsSbN was found to be kinetically limited in the range of 520-600 oC with an activation energy of 10.4 kcal/mol.

Figure 16. Growth rate of GaAsSbN as a function of growth temperature.

The growth rate is linearly related to the flow rate of the TMGa (figure 17) allowing precise control of layer thickness. However, the growth rate behavior is not fully described by the group III flux, which is another indication of kinetically-limited growth, as varying the group V flows also changes t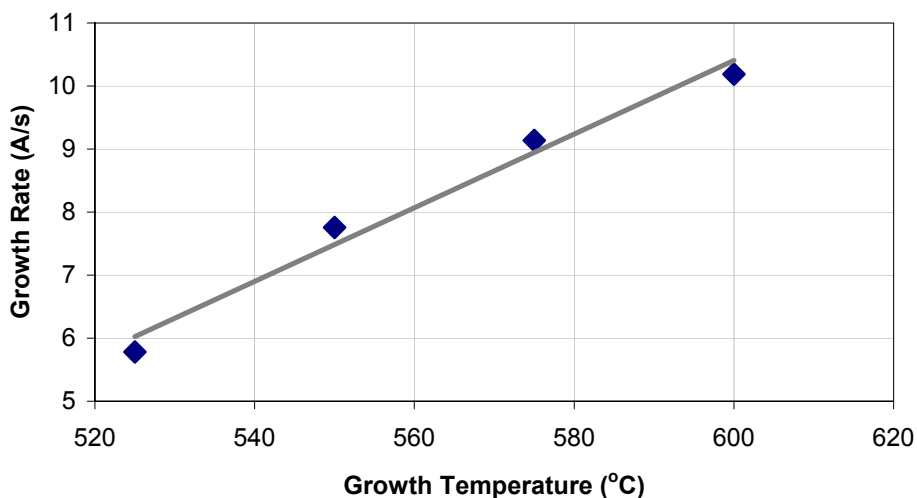he growth rate. The growth rate vs. group V behavior of this mixed anion quaternary is complex (figure 18) and involves chemistry that is not well understood at this time. In the ternary, GaAsSb, As is preferentially incorporated into the solid, and for GaAs(1-x)Sbx with x < 0.1, the growth rate increases monotonically with increasing AsH3 flow. [6] Figure 18 shows the growth rate of GaAs(1-x-y)SbxNy with x < 0.1 a) increasing linearly as the AsH3 flow is increased (with fixed DMHy and TMSb flow), b) decreasing linearly as the DMHy flow is increased (with fixed AsH3 and TMSb flow), and following a nonlinear, decreasing behavior with c) increasing TMSb flow (with fixed AsH3 and DMHy flow) and d) V/III ratio. This is similar to the behavior in GaAsSb, but there is additional passivation of the growth rate due to increased DMHy flow.
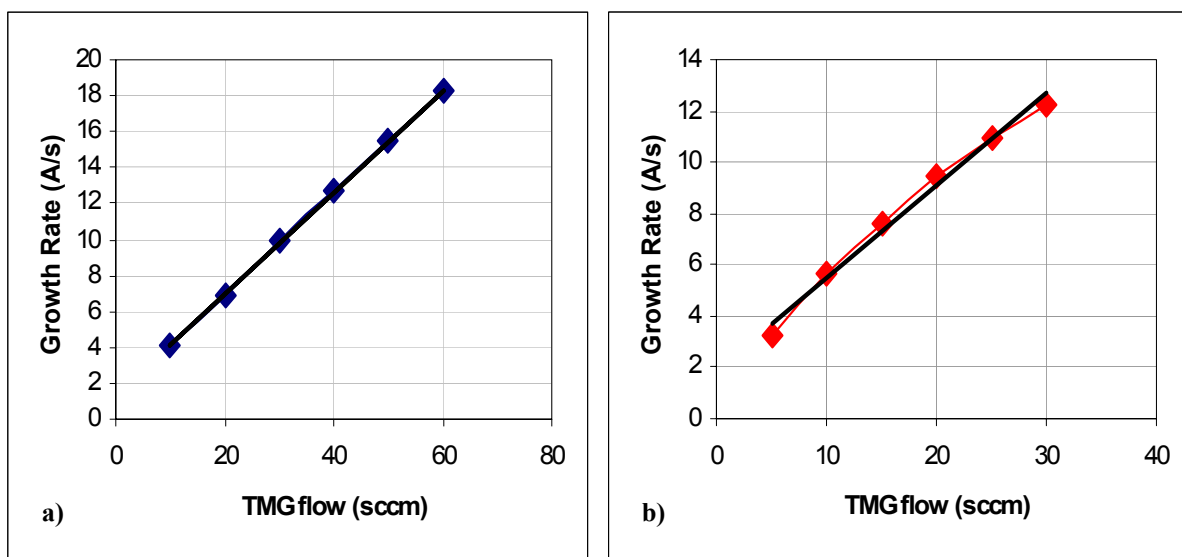

Figure 17. Growth rate of GaAsSbN as a function of TMG flow for a) fixed DMHy, TMSb and AsH3 flows, and b) fixed V/III ratio.
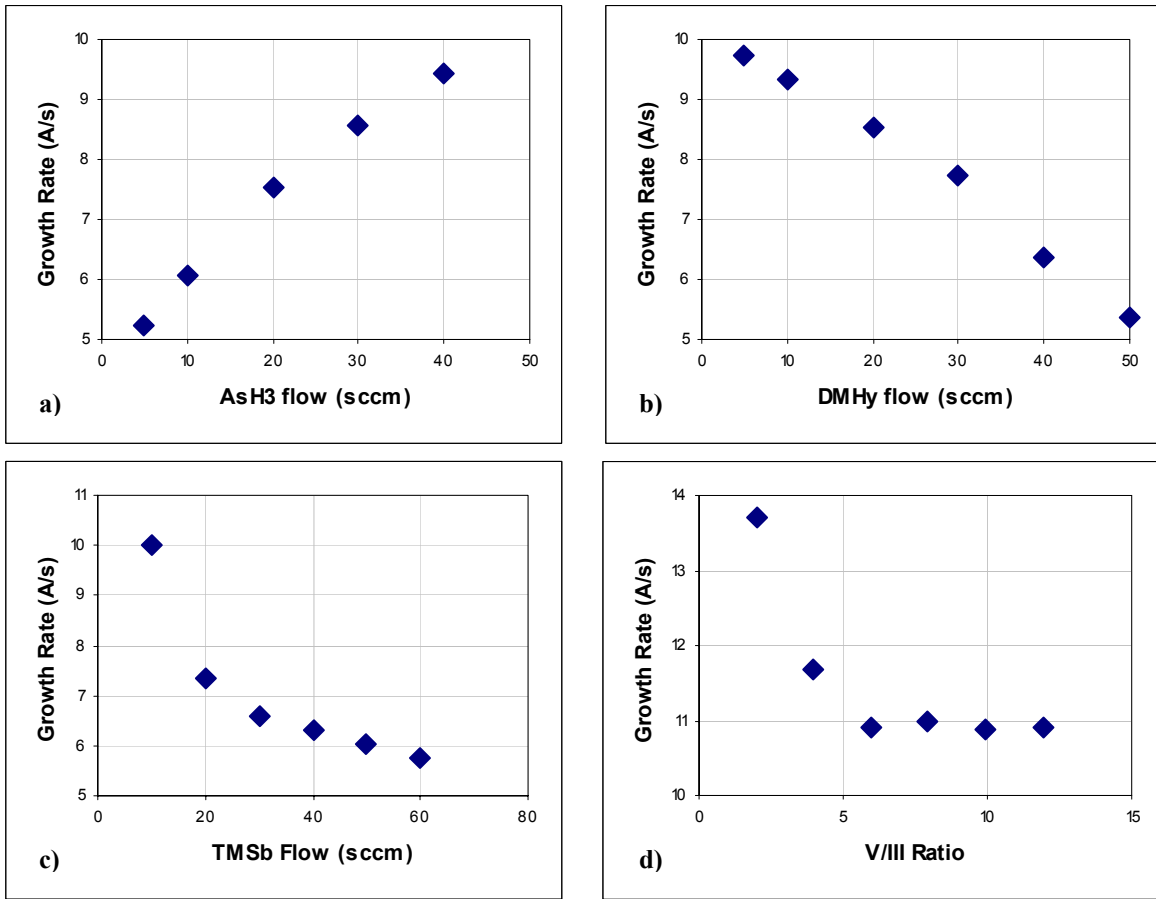
Figure 18. Growth rate as a function of the Group V constituents
a) AsH3 flow, b) DMHy flow, c) TMSb flow, and c) V/III ratio.

A higher incorporation efficiency of N in GaAsSbN has been reported for MBE, [7], in GaAsN and AlGaAsN for CBE [8], and in GaAsN for OMVPE [9, 10, 11] over InGaAsN. We have also observed this trend in our growths of GaAsSbN where we use flows of 30-50 sccm for 1% N, while typical flows for a similar concentration in InGaAsN are 350-600 sccm for material with 1.3 µm emission. This reduces the need for emissivity-corrected pyrometry to ensure proper wafer temperature for GaAsSbN growth since there is less surface cooling due to the lower flows.

3.3 GaAsSbN Quantum Well Studies

The growth conditions for long wavelength GaAsSb quantum wells were established at the lower temperatures necessary for N incorporation. Strained layer superlattices of GaAsSbN/GaAs were grown to determine interface quality and estimate the amount of antimony and nitrogen incorporation. Room temperature (RT) photoluminescence (PL) and X-ray diffraction (XRD) studies confirmed excellent material quality with antimony concentrations of 23% to 32% and nitrogen incorporation near 1%. A very narrow range of temperature (within 5%) and Sb/V ratio (0.3-0.35) has produced bright room temperature PL.   Incorporation of small amounts of nitrogen degrade the room

temperature photoluminescence. Increasing temperature during growth increases the emission wavelength at the expense of intensity and FWHM as shown in Figure 19.
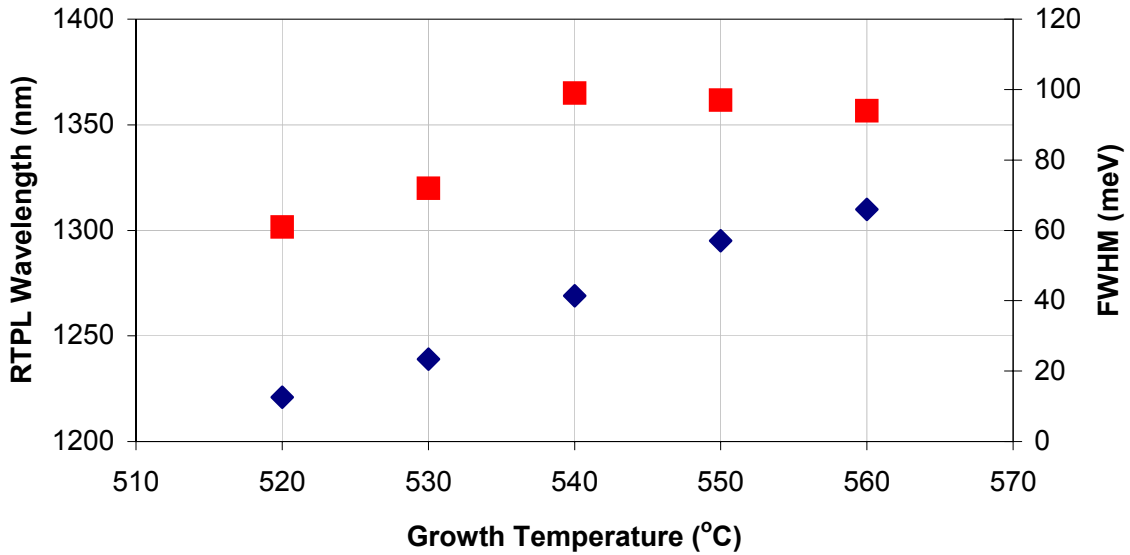
Figure 19. **Room temperature photoluminescence**
and full width half maximum as a function of growth temperature.

There is a very small range of temperature and V/III ratio that allows incorporation of nitrogen into the sample. As the temperature is increased, the GaAsSbN photoluminescence peak shifts to longer wavelength indicating that more N is incorporated into the sample (figure 19). This is contrary to the behavior in InGaAsN where increased temperature results in lower nitrogen incorporation. The shift in photoluminescence peak could be caused by higher Sb content; however, the XRD shows comparable Sb concentrations for all of these samples. Unfortunately the FWHM and intensity of the PL is degraded for the higher temperature growths. XRD of superlattice structures indicates that this is due to interface diffusion or roughening.

Low temperature (4K) photoluminescence of GaAs0.69Sb 0.3N0.01 shows a red shift of 55-77 meV, an increase in FWHM of 2.4-3.4 times the FWHM, and a decrease in intensity of one to two orders of magnitude as compared to GaAs0.7Sb0.3 (figure 20).

Figure 20. Low temperature (4K) photoluminescence of 40, 60, and 80 Å quantum wells of a) GaAsSb/GaAs and b) GaAsSbN/GaAs.
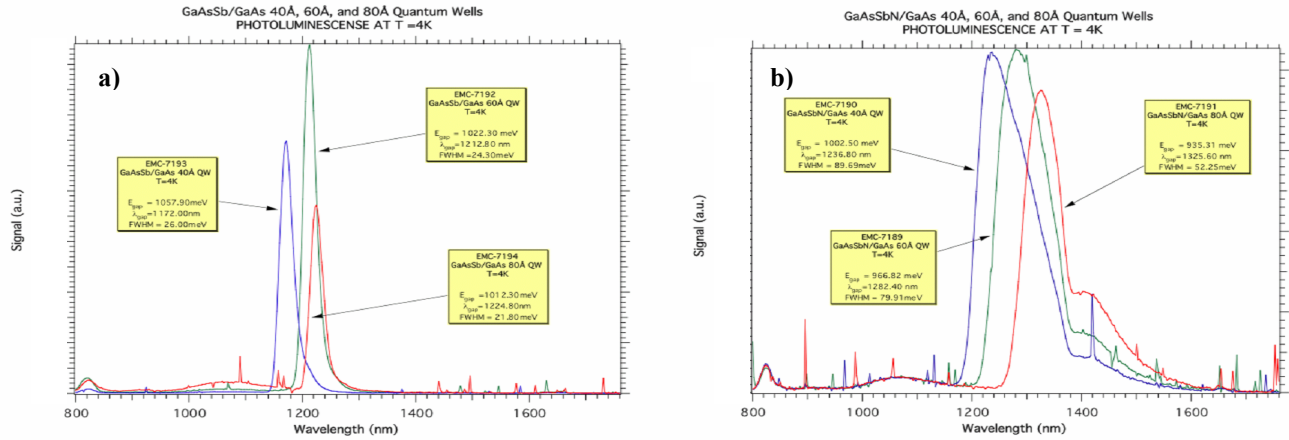
The 4 K photoluminescence spectra for 40, 60 and 80 Å GaAs0.7Sb0.3 QWs are shown in Figure 20 a). The addition of N to samples grown under similar conditions induces a 55-77 meV red shift as illustrated in Figure 20 b). The photoluminescence intensity of the GaAs0.69Sb 0.3N.01 samples is roughly 100x weaker than the non-nitrided samples, which is comparable to the behavior of InGaAsN. The FWHM of the GaAsSbN QWs is 2.4-3.4X greater than that of the GaAsSb QWs and there appears to be a defect related peak on the right shoulder that increases in intensity with increasing QW thickness. There is, however, less variation in intensity with QW thickness for GaAsSbN.

Figure 21 illustrates the annealing behavior of the OMVPE GaAsSbN. We have not seen a dramatic improvement in either 300K or 4K photoluminescence by any ex -situ annealing conditions from 600-825 oC for times less than 1 minute and using N2 ambient. In fact, for extreme annealing conditions of 825 oC for 10 seconds, a blue shift of about 55 meV is observed in the nitrided samples with a decrease in the FWHM of about 9 meV, while a blue shift of about 40 meV is observed in the samples without nitrogen with very little change in FWHM. The photoluminescence intensity of the GaAsSb sample decreased about three times along with this shift, and XRD indicates a loss of Sb in the QW region. Similar high temperature annealing of OMVPE grown InGaAsN can cause a much larger blue shift. So the major factor in the blue shift of the annealed GaAsSbN does not seem to be related to improvements to nitrogen caused defects or bond rearrangement. We attribute the reduced blue shift during annealing to the single group III chemistry.
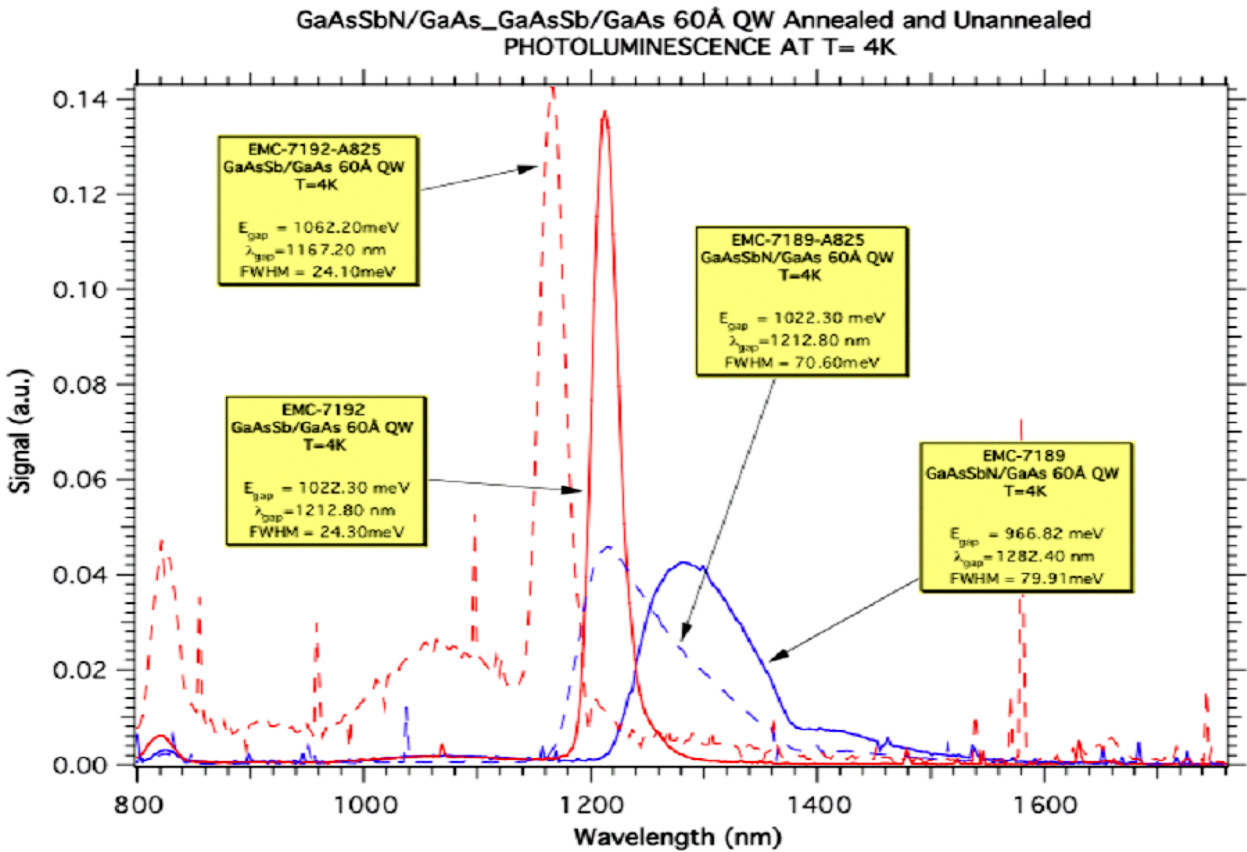
Figure 21. Low temperature (4K) photoluminescence of the annealing behavior of GaAsSb and GaAsSbN.

3.4 Transport Properties of GaAsSbN

GaAsSbN exhibits a small reduction in hole mobility as compared to GaAsSb. Cooper et al. [12] and Bedair et al. [13] reported mobilities near 500 cm2/V-sec for GaAs0.8Sb0.2 on GaAs with net carrier concentrations in the mid-1016/cm3. The mobility of nearly lattice matched GaAs0.94Sb0.05N0.01 at 300K was measured to be 350 cm2/V-sec with 1.0E17/cm3 background hole concentrations and the mobility at 77K was 1220 cm2/V-sec with a background hole concentration of 4.8E16/cm3. Interestingly, GaAsSb mobilities nearly lattice matched to InP are much lower than this at < 70 cm2/V-sec [14, 15, 16] and this has been attributed to alloy scattering and ordering effects.

An estimate of the carrier masses may be obtained by plotting the 4 K PL energy as a function of the inverse of the well width squared as illustrated in figure 22. In the GaAsSb/GaAs system, the electron experiences little or no confinement, so as the quantum well width is increased, the changes in the bandgap energy arise from the change in the position of the energy of the heavy hole state and the slope is proportional to the hole effective mass. The GaAsSbN/GaAs system has nitrogen to provide confinement in the conduction band, and in this case, the slope should be proportional to just the electron mass, since the electron is much lighter than the hole. From the measurement in Figure 23, we calculate a hole mass of 0.37-0.40mo for GaAsSb, and we calculate an electron mass of 0.2 to 0.3mo for GaAs0.69Sb0.3N0.01. A similar calculation for In0.07Ga0.93As0.97N0.03 yielded electron masses of 0.15mo. [17]
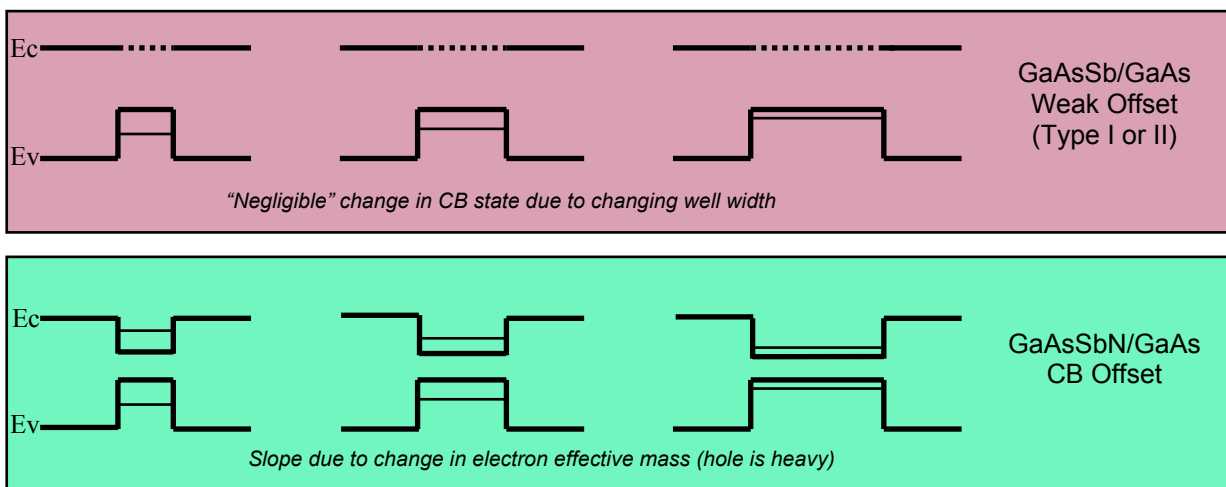

Figure 22. Simple model of electron and hole confinement in GaAsSb and GaAsSbN.
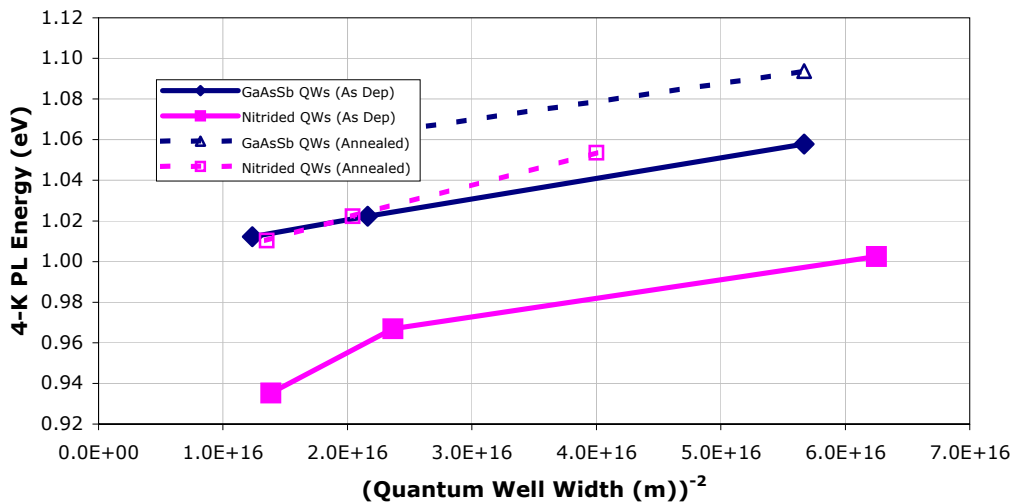

Figure 23. Measurement of the photoluminescence energy vs. inverse quantum well width squared.

4. Molecular Beam Epitaxial GaAsSbN materials

MBE growth provided many insights into the material properties of GaAsSbN. Our MBE GaAsSbN has produced one of the longest emission wavelengths of any type-I material ever grown coherently on GaAs substrates. We also produced the first estimation of the exciton reduced mass in GaAsSbN by measurement of the diamagnetic shift vs. magnetic field.

As a prelude to optimizing the growth conditions for GaAsSbN, we have investigated the effects of various growth conditions on the simpler ternary alloy GaAsSb to find appropriate limits to the parameter space to study for the N-containing alloys. Figure 24 shows room-temperature photoluminescence (PL) for a series of GaAsSb (6 nm)/GaAs quantum wells grown at various temperatures. Samples grown over the range 410-490ºC show clear trends including increasing intensity and increasing linewidth with increasing temperature. In addition, a slight shortening of the peak wavelength at the highest temperature is observed. The wavelength reduction has been previously observed, and is believed to be a consequence of Sb desorption, which becomes substantial above 490ºC. At lower temperatures, the reduced PL intensity appears to be a result of an increased density of non-radiative point defects. Because the GaAsSb alloy is itself immiscible for compositions with nearly equal Sb and As concentrations, we believe that the somewhat narrower linewidths at low temperatures reflect reduced phase separation between As-rich and Sb-rich regions of the alloy. Given the significant degradation of PL quality of the GaAsSb alloys at low temperatures, we believe that temperatures of approximately 390-490ºC were appropriate for investigations of the GaAsSbN alloy.
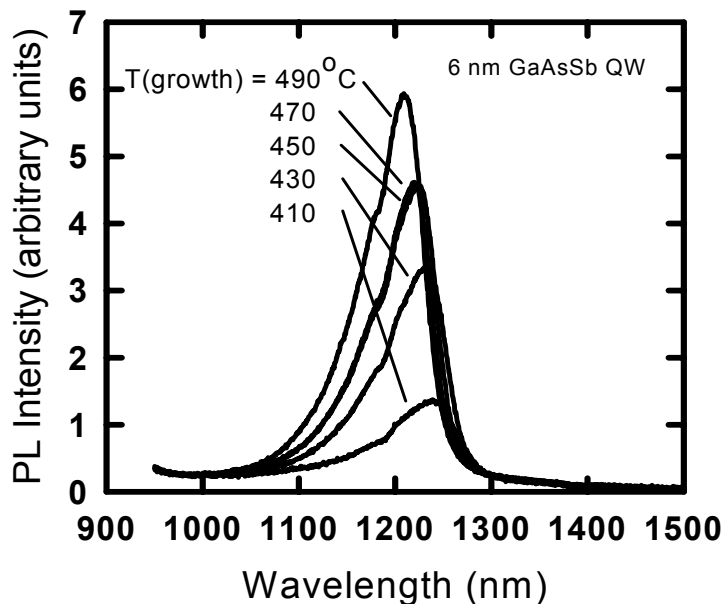

Figure 24. Room temperature photoluminescence of GaAsSb/GaAs quantum wells grown at various temperatures.

N-containing alloys were grown using reactive N species supplied by an RF plasma source attached to the MBE growth chamber. Pure N2 was used as the source gas, and plasma source operation was near the lowest RF power, which would sustain a bright plasma. In contrast to MOCVD-grown materials, N species have a high sticking coefficient in dilute-nitride MBE growth.

4.1 Low Nitrogen Concentration GaAsSbN

Initial studies were performed using N concentrations of approximately 0.1-0.2%. These relatively small concentrations of N resulted in a significant reduction in the room-temperature photoluminescence intensity relative to N-free samples. Figure 25 shows room-temperature PL for otherwise similar GaAsSb and GaAsSbN samples.
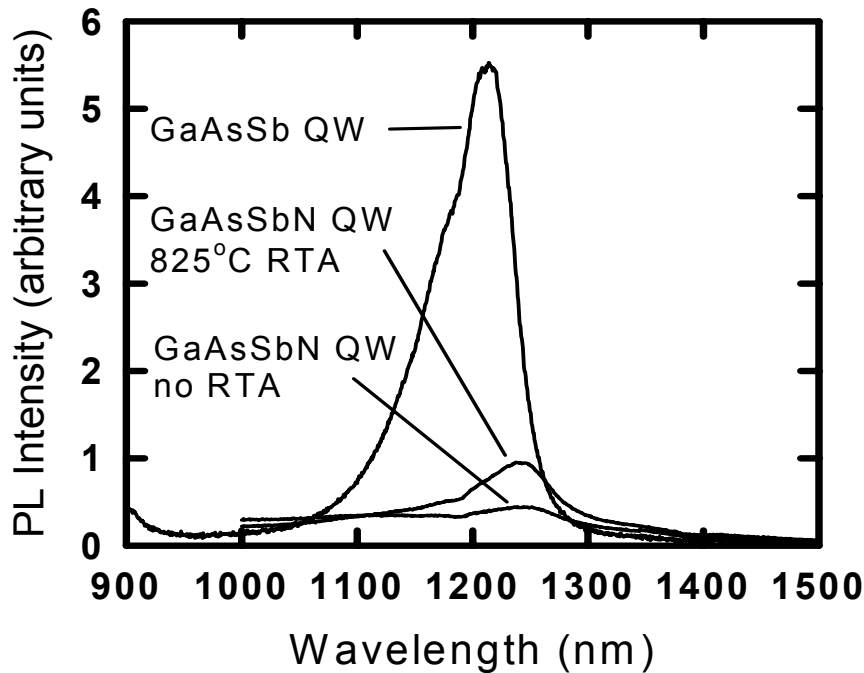

Figure 25. Room temperature photoluminescence from GaAsSb/GaAs and GaAsSbN/GaAs with low nitrogen concentrations.

As observed with InGaAsN alloys, post-growth rapid thermal annealing produced a substantial improvement in the PL intensity of the GaAsSbN. Based on a series of annealing experiments with these low-N samples, the optimum annealing temperature of approximately 825ºC is significantly lower than found for InGaAsN. Material annealed in this manner has a peak PL intensity, which is a factor of 5-10 weaker than similar GaAsSb, with a red shift of the bandgap of less than 50 nm.

4.2 High Nitrogen Concentration GaAsSbN

Quantum wells with substantially higher N concentrations have correspondingly weaker room-temperature PL characteristics, but nevertheless exhibit relatively bright and narrow PL at lower temperatures. Figure 26 shows 4K PL for GaAsSbN/GaAs quantum wells containing ~2% N and a N-free structure for comparison. For the unannealed

GaAsSbN structure, the peak of the PL signal occurs at approximately 1660 nm, representing a red shift of 400 nm (240 meV) relative to the N-free structure. Upon RTA, the PL emission intensity increases by a factor of >10, and the wavelength blueshifts to approximately 1530 nm, which still represents a redshift of nearly 300 nm relative to the N-free sample. We believe these quantum wells to be among the smallest bandgap type-I materials ever grown coherently on GaAs substrates. In contrast to other recent results of long-wavelength emission obtained in highly strained surfactant-assisted growth, our GaAsSbN quantum wells also have strain values within the Mathews-Blakeslee limit, which may be a requirement for obtaining useful lifetimes in device applications. The quality of the luminescence obtained from annealed samples appears adequate for further experimental investigations of band offsets and bandstructure, and will in addition serve as a metric to enable continued improvement in the growth and annealing conditions.
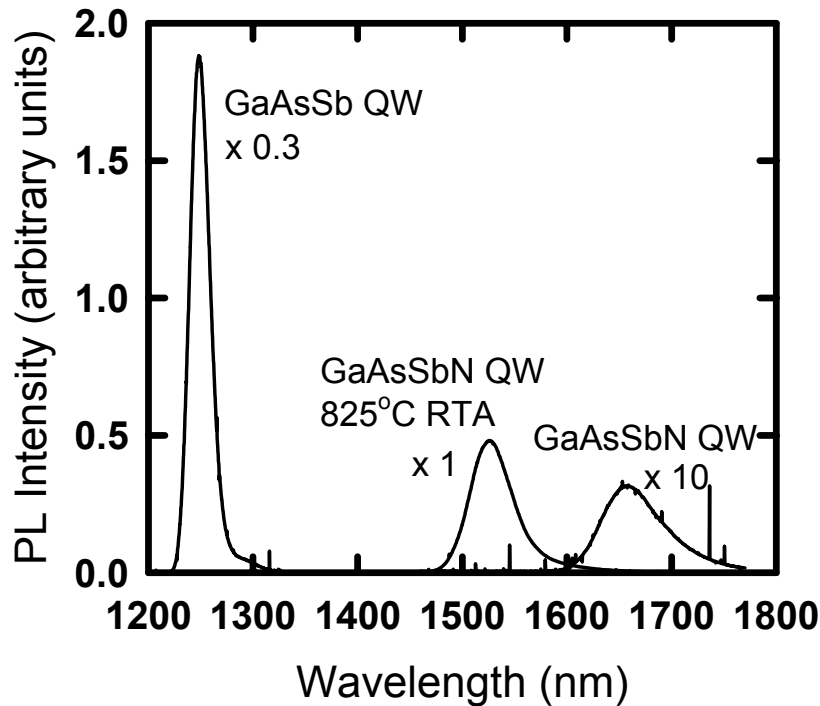
Figure 26. Low temperature (4K) photoluminescence from GaAsSb/GaAs and GaAsSbN/GaAs (large concentration) quantum wells.

4.3 Exciton Reduced Mass Measurement

A measurement of the diamagnetic shift vs. magnetic field was conducted at the National High Magnetic Field Laboratory at Florida State University in order to determine the exciton reduced mass for GaAsSbN. Both GaAsSb and GaAsSbN were measured under a magnetic field up to 35 Tesla. Figure 27 shows the results of this measurement.

Figure 27. The diamagnetic photoluminescence shift as a function of the magnetic field.
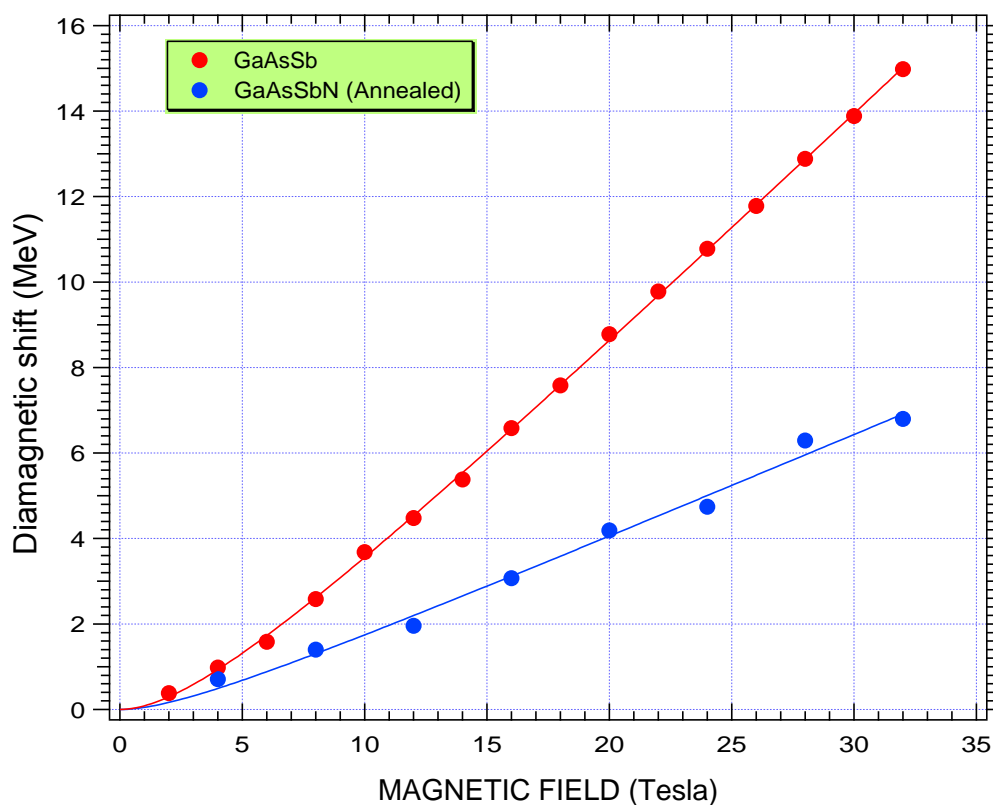
A comparison of the diamagnetic shift vs. magnetic field has allowed us to estimate the exciton reduced mass at two times the mass in the ternary GaAsSb.

5. Device Results

While InGaAsN has successfully produced lasers operating at or near 1.3 μm, it is difficult to produce lasers in this system with wavelengths longer than 1.3 μm. Furthermore, these lasers often suffer from poor reliability, high thresholds and poor slope efficiency at the present time. GaAsSbN active regions may be useful for lasers with wavelengths longer than 1.3 μm. We have only just begun to put GaAsSbN in laser cavities and the following is preliminary data of our first attempts.

A GaAsSbN active region was incorporated in an edge emitting structure to begin to determine the properties of an electrically injected device. Figure 28 is the CW electroluminescence data.
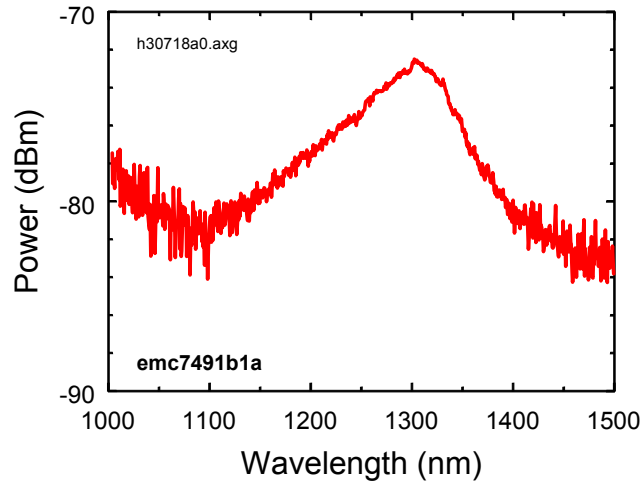
Figure 28. CW electroluminescence data from a GaAsSbN edge emitting laser.

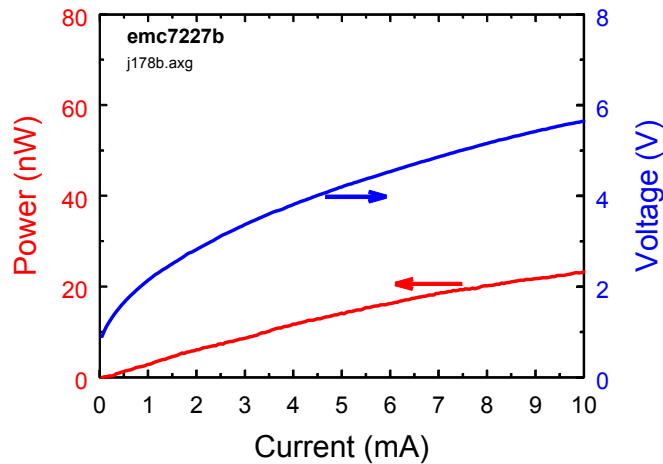We also introduced a similar active region into a VCSEL and figure 29 is the pulsed LIV data.

Figure 29. LIV data from a GaAsSbN VCSEL.

6. Conclusions

GaAsSbN has been comprehensively studied for the first time through theoretical and experimental investigation during this LDRD and has been identified as a superior candidate to B-based chemistries, and as a similar or potentially superior candidate to InGaAsN for long-wavelength applications. First principles modeling predicts that the addition of B to GaAs will decrease the emission wavelength, decrease the lattice constant and may have a higher tendency to form clusters. Furthermore, the three-fold degeneracy of the GaAs X-point is not lifted by the addition of boron, leading to a piecewise linear dependence of the bandgap on pressure, which results in forbidden optical transitions above the crossing of the gamma-like singlet and the X-like singlet. The addition of Sb to GaAsN increases the wavelength slightly more than the addition of In, however, the band gap fluctuations in the mixed anion nitrides arise primarily from the configuration of the nitrogen atoms. Clustering is also predicted to be more likely in the InGaAsN material system than GaAsSbN indicating that GaAsSbN may have advantageous transport properties to all three material systems. GaAsSbN was grown by both MBE and MOCVD well past 1.3 µm, with room temperature emission of > 1.4 µm for the OMVPE material and low temperature (4K) photoluminescence of the MBE material out to 1.66 µm which is one of the longest wavelength type-I materials ever grown coherently on GaAs substrates. The first measurement of GaAsSbN transport properties including low (77K) and room temperature mobilities, electron/hole masses and exciton reduced mass show behavior similar to InGaAsN. Devices were grown for characterization and electroluminescence was obtained at 1.3 µm. The GaAsSbN material system is now mature enough to be considered for numerous device applications as a direct result of this study.

References

E.D. Jones, N.A. Modine, A.A. Allerman, S.R. Kurtz, A.F. Wright, S.T. Tozer, and X. Wei, Phys. Rev. B 60 (1999) 4430.

S.B. Zhang and Alex Zunger, Appl. Phys. Lett. 71 (1997) 677.

R.R. Wixom, G.B. Stringfellow, and N.A. Modine, Phys. Rev. B 64 (2001) 201322.

R.R. Wixom, N.A. Modine, and G.B. Stringfellow, Phys. Rev. B, 67 (2003) 115309.

R.M. Biefeld, Mat. Sci. & Eng. Reports, 36 (2002)105.

S.M. Bedair, M.L. Timmons, P.K. Chiang, L. Simpson and J.R. Hauser, J. Electron. Mater., 12 (1983) 959.

J.C Harmand, G. Ungaro, L. Largeau, and G. Le Roux, Appl. Phys., 77 (2000) 2482.

J.O. Maclean, D.J. Wallis, T. Martin, M.R. Houlton, and A.J. Simons, J. Crystal Growth, 231 (2003) 31.

D.J. Friedman, J.F. Geisz, S.R. Kurtz, and J.M. Olson., J. Crystal Growth, 195 (1998) 438.

S. Kurtz, J. Webb, L. Gedvilas, D. Friedman, J. Geisz, J. Olson, R. King, D. Joslin and N. Karam, Appl. Phys. Lett., 78 (2001) 748.

T.Miyamoto, T. Kageyama, S. Makino, D. Schlenker, F. Koyama, and K. Iga, J. Crystal Growth 209 (2000) 339.

C.B. Cooper, III, R.R. Sexena, and M.J. Ludowise, J. Electron. Mater., 11 (1982) 1001.

S.M. Bedair, M.L. Timmons, P.K. Chiang, L. Simpson and J.R. Hauser, J. Electron. Mater., 12 (1983) 959.

B.T. McDermott, E.R. Gertner, S. Pittman, C.W. Seabury and M.F. Chang, Appl. Phys. Lett., 68 (1996) 1386.

R. Bhat, W-P. Hong, C. Caneau, M.A. Koza, C-K. Nguyen, and S. Goswami, Appl. Phys. Lett., 68 (7), (1996) 985.

S.P. Watkins, O.J. Pitts, C. Dale, X.G. Xu, M.W. Dvorak, N. Matine, and C.R. Bolognesi, J. Crystal Growth, 221 (2000) 59.

E.D. Jones, N.A. Modine, A.A. Allerman, I.J. Fritz, S.R. Kurtz, A.F. Wright, S.T. Tozer, X. Wei, SPIE, 3621 (1999) 52.

Distribution:

1	MS 9018	Central Technical Files, 8945-1
2	MS 0899	Technical Library, 9616
1	MS 0323	D. Chavez, LDRD Office, 1011
1	MS 0603	Gregory M. Peake, 1742
1	MS 0603	John F. Klem, 1742
1	MS 0603	Terry W. Hargett, 1742
1	MS 0603	Darwin K. Serkland, 1742
1	MS 0603	Michael J. Cich, 1742
1	MS 0603	Charles T. Sullivan, 1742
1	MS 1415	Normand A. Modine, 1112
1	MS 1415	Charles Barbour, 1112
1	MS 0601	Karen E. Waldrip, 1123
1	MS 0601	Steven R. Kurtz, 1123
1	MS 0601	Jerry A. Simmons, 1123
1	MS 0601	Andrew A. Allerman, 1126
1	MS 0601	Robert M. Biefeld, 1126
1	MS 0601	Eric Daniel Jones, 1123
1	MS 0601	Jerry A. Simmons, 1123